

Lappeenranta University of Technology
LUT School of Engineering Science
Degree Programme in Computational Engineering and Physics
Intelligent Computing Major

Vsevolod Radchenko

PROCESSING OF LONGITUDINAL RETINAL IMAGE SERIES

Examiners: Professor Lasse Lensu
Assoc. Prof. Mikhail Zymbler

Supervisor: Professor Lasse Lensu

ABSTRACT

Lappeenranta University of Technology
LUT School of Engineering Science
Degree Programme in Computational Engineering and Physics
Intelligent Computing Major

Vsevolod Radchenko

Processing of Longitudinal Retinal Image Series

Master's Thesis

2016

52 pages, 28 figures

Examiners: Professor Lasse Lensu

Assoc. Prof. Mikhail Zymbler

Keywords: image processing, medical imaging, retinal imaging, longitudinal series

A particular interest in medical image processing can be found in the case when a series of images captured at different time points from the same patient is provided for the analysis. This work focuses on the processing of such sets of retinal images called longitudinal image series. Several image preprocessing methods was considered in the application to longitudinal retinal image series, such as noise removal, image registration, and photometric correction. The impact of the latter technique on the further analysis was evaluated. A set of longitudinal image analysis techniques was also considered, including change detection and visualization, target segmentation, and change prediction. An experiment was conducted to establish possible regularities in the rates of the change occurrences throughout the dataset series. The experiment demonstrated that about 56% of the selected image sequences contain regions of blood vessels which widen with the equal rate between consequent time points.

ACKNOWLEDGEMENTS

First of all, I would like to express my sincere gratitude to my supervisor, Professor Lasse Lensu, for his patience and thorough guidance throughout all my work.

I am very thankful to my family for their constant support, from the moment I decided to participate in this endeavor till its last stages.

I would also like to thank my fellow students for the inspiring acquaintance and whole-hearted support during the studies.

This research would not be possible for me to conduct without the opportunity to take part in the Double Degree Programme provided by South Ural State University and Lappeenranta University of Technology. This programme was an exciting challenge and a very special experience.

TABLE OF CONTENTS

1	INTRODUCTION	6
1.1	Background.....	6
1.2	Objectives.....	7
1.3	Structure of the thesis.....	7
2	REVIEW OF LONGITUDINAL IMAGE ANALYSIS METHODS.....	9
2.1	Longitudinal analysis of retinal images	9
2.2	Techniques for change prediction.....	10
3	LONGITUDINAL RETINAL IMAGE DATASET	13
3.1	Dataset description.....	13
3.2	Processing of the image files and storage organization	14
3.3	Summary	15
4	IMAGE PROCESSING METHODS FOR CHANGE PREDICTION.....	16
4.1	Overall structure overview	16
4.2	Preprocessing pipeline	16
4.2.1	Noise removal.....	17
4.2.2	Image registration	19
4.2.3	Illumination correction.....	26
4.2.4	Color correction	29
4.3	Processing pipeline	31
4.3.1	Change detection and visualization.....	31
4.3.2	Vasculature segmentation.....	33
4.3.3	Morphology-based change prediction.....	34
5	EXPERIMENTS AND RESULTS	37
5.1	Impact of photometric correction techniques on change detection	37
5.1.1	Color correction	37
5.1.2	Illumination correction.....	39
5.1.3	Color correction combined with illumination correction	40
5.2	Morphology-based change prediction.....	41

5.3	Estimation of change pace.....	44
5.4	Discussion	46
5.4.1	Photometric correction	46
5.4.2	Change prediction	47
5.4.3	Notes on desired features of the longitudinal retinal image datasets.....	48
6	CONCLUSIONS.....	49
	REFERENCES.....	50

1 INTRODUCTION

1.1 Background

The first steps in the field of computer vision were made back in the 1970s, and this field has become extensive, providing an immense number of versatile tools currently applied in various fields. The invention of computer tomography and magnetic resonance imaging in medicine denoted the escalating interest in the approach of non-invasive study, and, as computational power of computers was increasing, such techniques became commonplace also in practical medicine.

Eventually, the algorithms of computer vision have been applied to image analysis in medical sciences. For example, in ophthalmology, they are applied to the retinal image analysis for diabetic retinopathy diagnostics. The disease remains one of the leading causes of blindness [1], even though such consequences could be alleviated if a patient is provided with proper care and preventive monitoring [2]. It has been demonstrated that the application of image processing algorithms for automatization of diabetic retinopathy diagnostics not only beneficially impacts the ratio of correct diagnoses at the early disease stages, but is also financially efficient [3].

Diabetes is associated with visible abnormalities in the retinal images. They include, for example, lesions growth, texture change or vasculature structure change. A significant proportion of such changes are of longitudinal nature, that is, once detected, they can be traced through time. This aspect reveals a particular approach for diagnostics, as it is a common practice for the patients with chronical diseases (such as diabetes) to perform medical check-ups on a regular basis, thus providing valuable longitudinal information about their health.

The longitudinal information may also include a set of retinal images, taken at different time points. To analyze them, a specially designed image analysis techniques could be applied, as it is not a single image of a patient's retina which is available, but a time sequence of images. Namely, an image series can be considered as a function of time, allowing to study this function by tracing the changes occurring in the images as the time passes.

1.2 Objectives

The target dataset of this thesis contains the longitudinal series of retinal images for a considerable number of patients. The motivation for this study is to construct a system for the utilization of the longitudinal information contained in these images to predict changes in these series. However, the process of actual longitudinal study must be preceded with a pre-processing pipeline pertinent to the longitudinal nature of the dataset. Consequently, the primary goal of this work can be expressed in the two following objectives:

- Assemble the preprocessing pipeline to prepare the retinal image series for the analysis.
- Apply a technique for processing of longitudinal image series to predict changes in the series of the given dataset.

To achieve the stated objectives, the following tasks must be addressed:

- Understanding of the dataset: the nature of the contained images must be studied.
- Image-wise preprocessing: the images must be cleared from the noise.
- Preprocessing of image series: the images contained in the sequences must be presented in a uniform way, including both geometry and color characteristics.
- Longitudinal change study: the changes occurring in the images during the timeline must be displayed and utilized for prediction purposes. The impact of the chosen preprocessing techniques to the change detection must also be evaluated.

An important limitation is the restriction to the target dataset: as there are no other longitudinal retinal images datasets openly available, the only images that can be considered are the ones from the given dataset.

1.3 Structure of the thesis

The thesis is composed of the introduction, four chapters, conclusions, and a list of references.

Chapter 2 is a literature overview of the field of longitudinal image analysis.

Chapter 3 contains the overview of the target dataset and describes the nature of the images contained in it. The preparation steps that were undertaken to prepare the images for the image preprocessing algorithms are described.

Chapter 4 presents the pipeline for the processing of the longitudinal image sequences. The design of the suggested cascade of algorithms is described. The image preprocessing steps that were overtaken to prepare the dataset for longitudinal analysis are described. The motivation behind these steps is explained, and the methods' overviews are provided. Finally, the processing techniques that were applied to the images as to longitudinal series are described, including primary processing of longitudinal image series and the actual change prediction.

Chapter 5 presents the experiments performed on the dataset. The impact of an image pre-processing technique is evaluated. An experiment to test the efficacy of the assembled pipeline is described. It also denotes the desired qualities of potential longitudinal retinal image datasets.

In the conclusions chapter the work is summarized.

2 REVIEW OF LONGITUDINAL IMAGE ANALYSIS METHODS

2.1 Longitudinal analysis of retinal images

The analysis of medical images has recently become a wide-spread study topic. Some of the works target exactly the case of several images available for the analysis, instead of the case of a single image.

The work [4] is one of the earliest articles which target processing of longitudinal retinal image series. The focus of the work is drusen segmentation and evaluation of its longitudinal changes among series of three images. The eventual system is semi-automatic: the automatic part is lesion segmentation, though supplemented by a possibility of manual control. Assessment of the longitudinal changes is essentially visual.

In comparison with the data set from the article [4], it can be observed that if it is lesions that affect the retinal image of the target dataset of this work, they most commonly occur in the latest image of the series, with no precursors in the previous ones.

It is also important to mention that in work [4] the preprocessing pipeline does not include series-wise preprocessing steps: the correct alignment of the images and uniformity of illumination are taken for granted. It, again, may be due to the nature of the images from the dataset considered in this paper, but such assumptions cannot be made in the case of the target dataset of our work.

The work [5] provides a supportive ground for the adaptive optics for retinal imaging. Its focus is change detection in retinal image series obtained during infrared imaging. This technique is used in laser treatment systems for pathology sensing, in order to prevent the laser from hitting the healthy retinal area. The risk is increasing in the case of a moving retina, so the change detection system is proposed to trigger the laser off. The primary challenges here are illumination changes and background noise which confuse the retinal motion detection process.

A straightforward subtraction of the subsequent frames cannot be applied to the discussed case due to illumination and noise variations. Instead, the authors of the paper utilize an approach based on the information theory, using gradients to represent the local information.

It is important to outline the difference of the data considered in our work from the one discussed in the abovementioned article. A unit of the former dataset is a series of three images in average, whereas infrared image sequences can be thought of as videos of hundreds of frames. The different amounts of data in the datasets contain the different potential for the longitudinal analysis.

The work [6] is dedicated to the assembling of a complete pipeline for retinal image preprocessing, change detection among the series and the classification of the changes. The article underlines the necessity of uniformity among the retinal images for change detection and processing purposes. It describes in detail the required algorithm cascade for the purpose. The primary steps of the cascade are image registration and illumination correction. These steps were implemented manually and were preceded by the steps of detection of significant regions of retinal images, namely, vasculature, optic disc, and fovea. The areas were segmented out so that the rest of the image would contain only the smoothly illuminated background, and then the vasculature information was used for the registration.

The preprocessing part is followed by the Bayesian change detection and classification. The implemented system was executed over a dataset specially assembled for the purpose in a medical institution, using a fundus camera with the beforehand known settings. The experiments demonstrated that the designed system is consistently reliable.

The problems considered in the article [6] and the nature of its target dataset are very close to the ones of this thesis. The primary difference is the longitudinal nature of the target dataset of this work, but it does not change the required preprocessing steps. Taking this into account, it was decided to design the preprocessing part following the article.

The work [7] is an improvement of the work [6], adding the separate consideration of the changes in blood vessel structure, such as width or an appearance of a new vessel, and the other changes.

2.2 Techniques for change prediction

From the viewpoint of prediction of pathology advancement in longitudinal series of medical images, the work [8] appears to be efficiently representative. It is dedicated to the construction of a system for tumor growth prediction based on image series depicting the kidney

tumor. According to the review performed by authors of the work, the work is novel and is the first to fulfill the task of kidney tumor prediction. To model the kidney tumor spreading, the reaction-diffusion model [9] was chosen.

The core functionality of the system is represented by common machine learning steps of training, prediction, and validation: having a longitudinal series of $n+1$ images, the last one of them is left out, and the rest are used for the estimation of parameters of the tumor growth model. Based on the estimation, the next image in the series is predicted and then validated by comparison with the initially left out image.

The training of the parameters itself is preceded by image preprocessing. Firstly, the images from the target set are registered. Next, the kidney segmentation is performed, being followed-up by the segmentation of specific areas of interest such as tumor regions. Lastly, the segmented tissues are meshed.

The experiments in this work were performed on the sequences of seven time points. The figures of the quantitative evaluation of the proposed system's accuracy are described as 'quite good' and proving the efficacy of the approach.

Another recent paper dedicated to tumor progression prediction also utilizes the texture-based mathematical model for the machine learning [10]. To improve the tumor growth prediction, the authors propose to fuse the tumor growth model and a novel tumor segmentation method based on super-pixels [11]. To accumulate the results the joint label fusion algorithm was used.

The Kalman filter is also widely applied for such purposes in medical imaging [5], [12]–[14]. Its most common use case is in videos or other continuous sources of images.

It is important to outline the major difference between the study environments in the above-mentioned cases and the target dataset of this work. While the works utilizing machine learning techniques are provided with the rich possibility for learning purposes, in our case we are restricted to only three time points for a series. It could be an option to target some specific changes, but since the dataset is not of such nature, it is also infeasible: the patients depicted in the dataset experience various conditions, with no pattern of occurring for some

specific signs of these conditions. Being restricted, it was decided to proceed with an approach which utilizes only the information in the current image.

The work [15] considers the case of medical imaging related to so-called volumetric images which are datasets composed of slices of an imaging target. The images of this kind are obtained, for example, from MRI. The paper targets the application of morphology-based methods to perform interpolation between two successive slices. In contrast to the machine learning approach, morphology operators work only with the information given in a target image, and no other images, which fits the restrictions of the target dataset.

3 LONGITUDINAL RETINAL IMAGE DATASET

3.1 Dataset description

There are several openly available retinal image datasets, for instance, REVIEW[16], DRIVE [17], STARE [18], or DIARETDB [19]. Such databases were created to serve various purposes, such as vasculature extraction or detection of signs of specific eye-related diseases such as diabetic retinopathy. Furthermore, some of the sources considered in this work make an extensive use of databases collected locally, usually provided by local hospitals.

The most distinctive feature of the considered dataset is a possibility to trace longitudinal changes occurring on the human retina as the time passes. To the best knowledge of the author, the dataset is the only one available for such purpose.

The nature of the dataset is thoroughly described in the article on the corresponding ophthalmological study [20]. Its contents are apparently altered from the point of the study publication, namely, some image sequences were added. The changes are not crucial, as the supplementary sequences hold the same longitudinal imaging properties.

The provided dataset contains the retinal images taken from 88 patients in different years with the interval of 5 years. Images of both the left and right eyes were taken from almost every patient, with irregular exceptions. An image series for an eye of a single patient consists of three images taken at three different time points. The small number of the time points in the sequences turned out to be a crucial restricting factor for the choice of the longitudinal image analysis approach.

The properties of the images even inside a single time series are not consistent. Namely, image series consist of grayscale and color images with varying geometric locations of a retina on the frame. Such inconsistencies occur in patterns justified by the changes of the imaging equipment and the imaging setups. Different cameras were used for capturing of the first image of the sequences and of the last two images. Additionally, at different time points, the cameras were set up for different angles of the capturing fields and for the different color ranges.

The images were complemented with the information regarding the patients' names, years of image takings and which side of the eye an image depicts. The patients are known to be diagnosed with type 2 diabetes. Otherwise, they have varying medical background: the dataset includes the photographs captured from men and women, with different smoking and medicine usage histories.

An example of three different time series is presented in Figure 1.



Figure 1. An example of three time series from the target database. Each row contains different time series captured from different patients.

3.2 Processing of the image files and storage organization

It should be noted that the supplementary information for the dataset contained a considerable number of mistakes such as index inconsistency. It most likely was caused by a large number of manually performed operations during the dataset composing.

The necessity of the primary step of the image files processing was justified by the most critical of the mistakes: the images filenames contained the names of the patients from whom the pictures were obtained. Such information must be strictly secured, and cannot be present

on the stages of image analysis. The first step of the filename processing thusly was making the images anonymous by removing the names of the patients and substituting them by indexes. Consequently, the second step was sorting of the images by the patients from whom they were acquired.

Even though these particular steps cannot be characterized by high complexity, a considerable amount of work time was dedicated to it. The primary reason for it was the necessity of manual fixing of the inconsistencies mentioned above which could severely flaw the dataset processing. For instance, a case in which an image from a series of a patient is erroneously named to be belonging to the series of another patient can bring undesired confusion to the routines of longitudinal image processing.

The dataset was composed out of 1342 images with a total size of 440 MB.

Due to the relatively small size of the dataset, its storage in a database was considered excessively complex for this work. The images were continued to be stored in files, with no additional architectural layers. The navigation through the images was organized by the file naming patterns which contained the patient's index, the year of the picture shooting, and the side of the eye. The file paths were exported into a MATLAB structure.

3.3 Summary

The database imposes quite strong restrictions. Firstly, even though the dataset contains several time points for each series of images, their number is very small for application of some longitudinal analysis techniques such as machine learning. Additionally, the variation of imaging conditions underlines the necessity of their preliminary preprocessing.

4 IMAGE PROCESSING METHODS FOR CHANGE PREDICTION

4.1 Overall structure overview

The considered problem of this work is developing of an algorithm cascade for the utilization of the longitudinal information contained in the time series of the target dataset for the change prediction purpose. After consideration of the nature of the target dataset and the relevant literature, the following algorithm was assembled for the processing of an image sequence from the dataset (see Figure 2). The method consists of the series preprocessing and series processing stages.

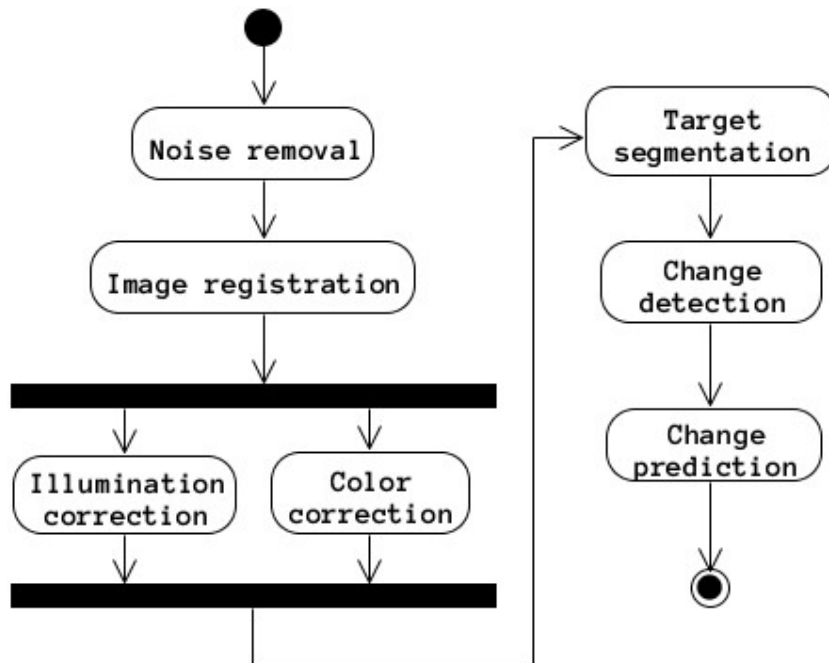


Figure 2. Activity diagram for the processing of an image series. The subsequence on the left side presents series preprocessing steps. The subsequence on the right side presents series processing steps.

4.2 Preprocessing pipeline

The purpose of the preprocessing pipeline is to prepare the image set for the extraction and utilization of the longitudinal information. This information is essentially contained in differences between the images of the series, so the priority is to prevent detection of erroneous

changes (caused, for example, by noise affecting some of the images) and to support the detection of semantically important changes.

The preprocessing pipeline falls into the following steps:

- Noise removal (or image-wise preprocessing): all the images must be cleared from any apparent side-effects originated not from the imaging process, such as occasional dust or markings.
- Image registration (or image alignment): in order to study the differences between the images, they should be aligned in such a way so that their contents are located at the same coordinates.
- Photometric correction: while image registration deals with the differences of geometric nature, the differences in coloring and intensities should also be handled not to mislead the change detection step.

4.2.1 Noise removal

4.2.1.1 Overview

As it was stated, the objective of the work is to study the changes occurring in longitudinal image series. It outlines the goal of the preliminary image enhancement which is supporting both the processes of image alignment and change analysis. The former process could be hindered, for example, by non-trivial geometrical distortions in the images, making a straightforward image registration impossible. The latter process could be hindered, for example, by a noise which is not consistent in an image series.

The range of noise removal techniques is very wide, including spatial domain techniques, frequency domain techniques [21], probabilistic models [22], or morphology [23]. In this thesis, the most popular technique of median filtering was used [21], as the salt-and-pepper type of noise is prevalent in the dataset. The median filter iterates through the image, replacing the value of each pixel by the median of its neighborhood.

4.2.1.2 Application to the target dataset

The images of the target dataset contain noise which originates not from the imaging process but rather from some mechanical alteration. Namely, the eye fundus slides were digitized using a scanner [20]. This resulted in the unintentional appearance of dust and dirt in some

of the images. Furthermore, most of the images contained annotations made by the authors of the dataset. Though useful for the understanding of image contents by an observer, these manual annotations present noise for image analysis.



Figure 3. An example of noise filtering. The top image depicts an image from the dataset. The bottom image presents the result of the median filtering. The red ellipses encircle the example areas where the noise removal occurred. The original image contrast was changed for the demonstration purpose.

The first stage of the image preprocessing was an automatic removal of the noise of this kind. In MATLAB, the median filter is implemented in the function `medfilt2()`. As certain classes of noise (such as the manual markings) appear quite regularly in the dataset, the noise removal was performed on all the images. An example can be observed in Figure 3.

4.2.2 Image registration

4.2.2.1 Overview

The nature of the retinal image dataset considered in this work is such that the photographs are taken at different time points. An important consequence of this point is the variance of geometrical properties of the photographs throughout series, even though the imaging target – human retina – remains the same. The primary reason for this is the usage of different imaging equipment at different time points. Namely, two different cameras were used for the imaging of the baseline and the imaging of the last two time points, as well as different fields around the fovea were photographed [20]. Furthermore, some variation is still possible even between the last two images of a series due to different positions of the same camera.

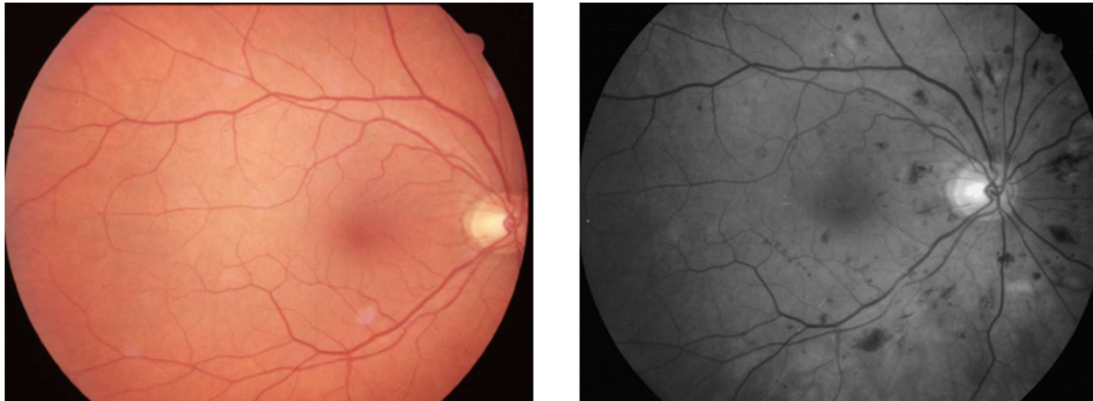


Figure 4. An example of the case of images captured at different timepoints and requiring proper alignment.

Figure 4 illustrates the problem. Both images were taken from the same patient but at different time points. It leads not only to different color information but also to the differences in the positioning: originally the images are of the same size, but the optic disc on the left image is in immediate vicinity of the border of the fundus ellipse, whereas the optic disc on the right image is considerably more distant from it.

To study the longitudinal properties of the image series, the images must be aligned in such a way that the objects in them are positioned in the same locations. It can be achieved by the image registration technique.

Image registration (also called image alignment [24]) is a machine vision technique for determining such geometrical transformation among a pair of images that its application would

result in spatial alignment of the subjects contained in these images [25]. From a mathematical point of view, image registration can be defined as a spatial mapping between two images [26]. For instance, defining two images I_1 and I_2 as a mapping $I(x, y)$ of pixel coordinates x and y to their intensity values, image registration between them, in the most general form, can be expressed in the following way [26]:

$$I_2(x, y) = g(I_1(f(x, y))), \quad (1)$$

where f is a coordinate transformation, g is an intensity transformation. Image I_1 , which is transformed to align with the image I_2 , is called a moving image or a floating image, and image I_2 – the unchanged one – is called a fixed image or a base image.

It is important to notice that the image characteristics can differ in some way, for example, they can be acquired at different time points or space points, or, in the case of medical imaging, they can even be acquired from different sources. Essentially, these characteristics justify the problem of image registration.

The knowledge of this machine vision technique is presented in a great range of scientific papers: the topic is widely presented in different surveys [26], [27], [25], [28]. Still, the structure of image registration algorithms commonly falls into the following algorithmic pattern:

1. Feature detection. To geometrically transform the first image according to the contents of the second image, it is necessary first to detect anchor points which are common to both images and which can be relied on as belonging to the same semantic object. This procedure can be performed either automatically or manually; automatic feature detection is a rich topic for scientific studies.
2. Feature matching. As features were detected, it is necessary to establish a correspondence between them.
3. Transform model estimation. Given an established correspondence between the feature points, the next step is creation of a mapping function that would establish a spatial relation between the images themselves.

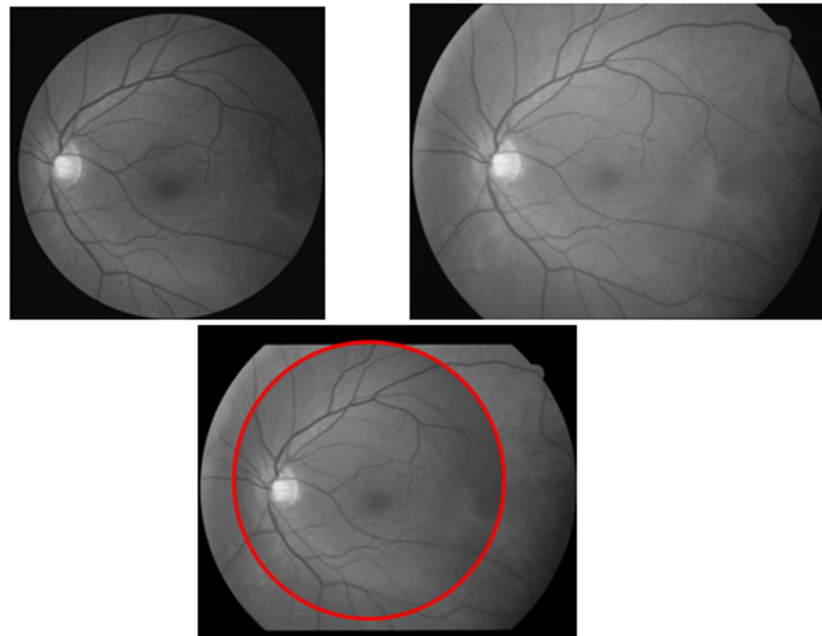


Figure 5. An example of image registration. The red ellipse highlights the border of the first image aligned over the second image.

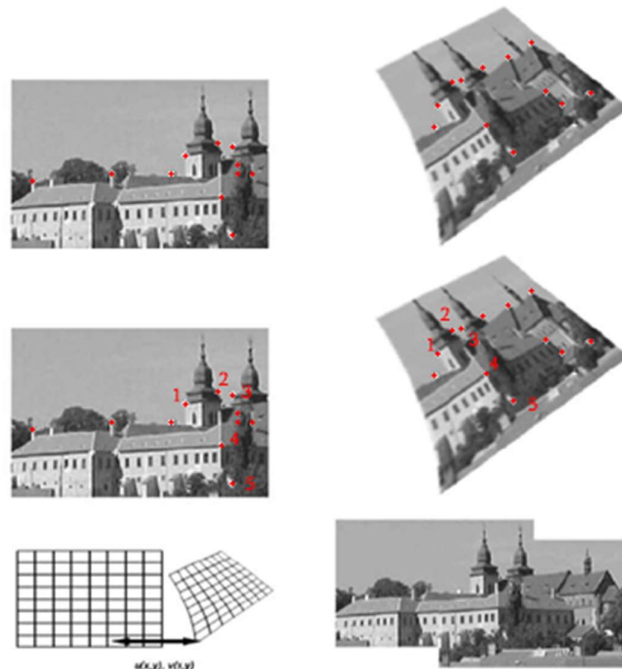


Figure 6. An illustration of the image registration process. The top row illustrates feature detection on the image pair, the second row – feature matching. The left image of the bottom row illustrates transform estimation, and the bottom right image depicts resampling of an image pair [27].

4. Image resampling and transformation. Given the mapping function, the rest to be done is to perform the final registering transformation.

The image registration steps are illustrated in Figure 6.

4.2.2.2 Generalized Dual-Bootstrap-ICP Algorithm

According to the survey [29], the Generalized Dual-Bootstrap-ICP (GDB-ICP) algorithm [30] was considered as the most applicable for registration of retinal images and was used in this work.

The structure of the algorithm described in the paper essentially corresponds to the above-mentioned pattern:

- Initialization: as the core principle of the algorithm is an iterative refining of a transformation model, the purpose of the initialization step is to provide an initial transformation.
- Estimation: The key part of the algorithm responsible for the reevaluation of the initial transformation model. When applicable, at this step the usability of other transformation models is also considered.
- Decision: it is required to determine which of the obtained estimates fits the best, or to declare that none of them can be used.

In this algorithm, the search for the keypoints is performed by calculation of local intensity gradients of an image, and the biggest magnitudes are considered most important and thus taken as an anchor point.

The drawback of such approach is that in the images where some kind of a border is present (for example, retinal border on retina images), it tends to take points from this border, ignoring semantically important parts from the rest of the image. It happens due to the relatively low value of the gradient. To override this, masks can be applied to the keypoint detection step.

The found keypoints are represented by scale-invariant feature transform (SIFT) [31] descriptor. Its primary purpose is to perform feature matching: two corresponding SIFT vectors from two images with the lowest Euclidian distance are considered to be matched. When

feature points are found, the algorithm next searches for the most appropriate model to describe the transformation which is the main output of the whole algorithm.

4.2.2.3 Geometric distortion correction

While the paper [30] suggests the usage of the quadratic transform to retinal images, this conclusion is not entirely applicable to our particular dataset, as some of the images among the series are taken by different imaging systems, involving different camera lens setups. Figure 7 demonstrates the issue.

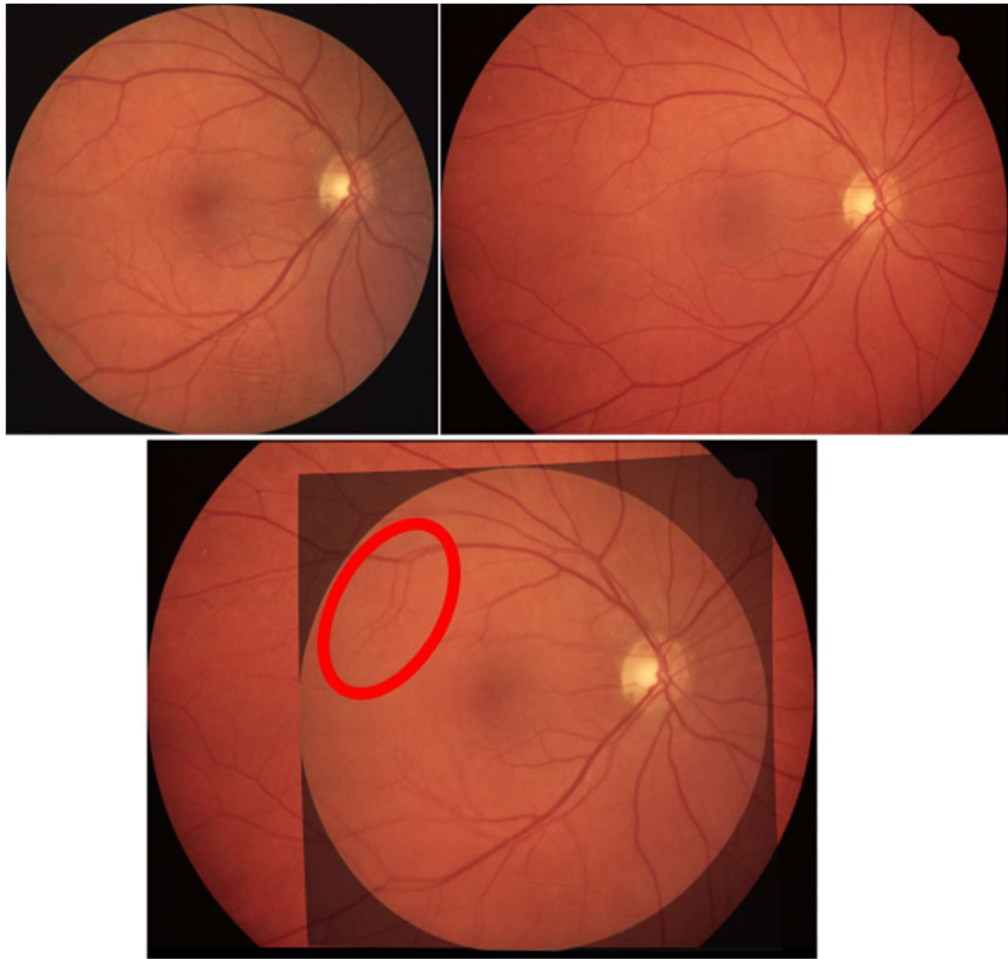


Figure 7. An illustration for quadratic transform application to the target dataset. The top images are the images from the same time sequence. The bottom image is the result of their registration through the quadratic transform. The red ellipse encircles an example of misalignment of vasculature.

To register such images, the GDB-ICP algorithm for estimation of a geometrical transformation along with lens distortion was used.

The transformation is written in the following way [33]:

$$\begin{bmatrix} q_x \\ q_y \end{bmatrix} - \begin{bmatrix} d_1 \\ d_2 \end{bmatrix} = D \left(T \left(D \left(\begin{bmatrix} p_x \\ p_y \end{bmatrix} - \begin{bmatrix} c_1 \\ c_2 \end{bmatrix}; k_1 \right); H \right); k_2 \right), \quad (2)$$

Where p_x, p_y are coordinates of the original point, q_x, q_y are coordinates of the point after the transformation, D is a radial lens distortion function, and T is a homography function. The radial lens distortion function is written as:

$$D \left(\begin{bmatrix} x \\ y \end{bmatrix}; k \right) = \left(1 + k \left\| \begin{bmatrix} x \\ y \end{bmatrix} \right\|^2 \right) \begin{bmatrix} x \\ y \end{bmatrix}, \quad (3)$$

The homography function in homogeneous coordinates is written in the following way:

$$T \left(\begin{bmatrix} x \\ y \end{bmatrix}; H \right) = \begin{bmatrix} (h_{11}x + h_{12}y + h_{13}) / (h_{31}x + h_{32}y + h_{33}) \\ (h_{21}x + h_{22}y + h_{23}) / (h_{31}x + h_{32}y + h_{33}) \end{bmatrix}, \quad (4)$$

H is 3-by-3 homography matrix. This matrix, along with the parameters $c_1, c_2, d_1, d_2, k_1, k_2$, is estimated by Levenberg-Marquardt's algorithm [6].

Consider Figure 8 for the illustration of the GDB-ICP registration.

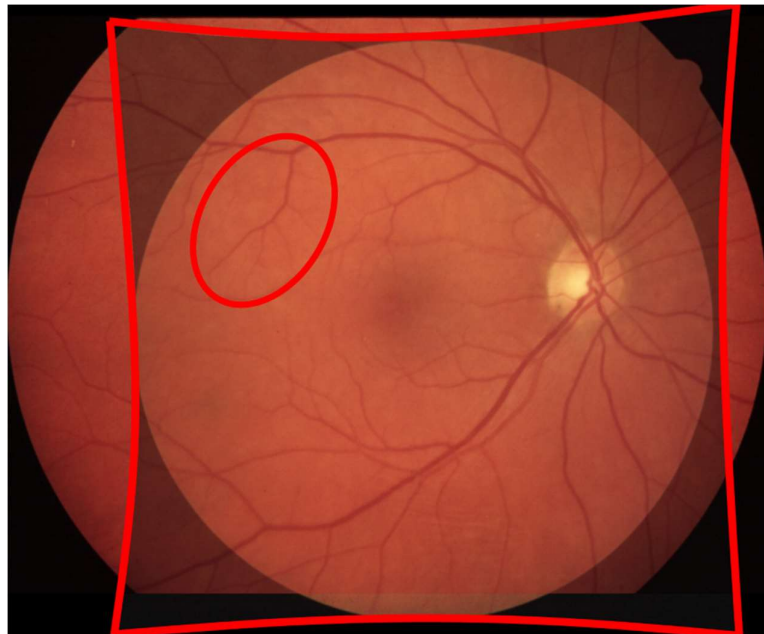


Figure 8. The result of GDB-ICP image registration with the transformation model of homography with lens distortion. The red ellipse encircles the same area as in Figure 7. The vasculature inside it is no longer misaligned.

4.2.2.4 Application to the target dataset

The GDB-ICP algorithm is provided as a ready-to-use executable which was utilized in this thesis. The result of the application of the GDB-ICP image registration is presented in Figure 9.

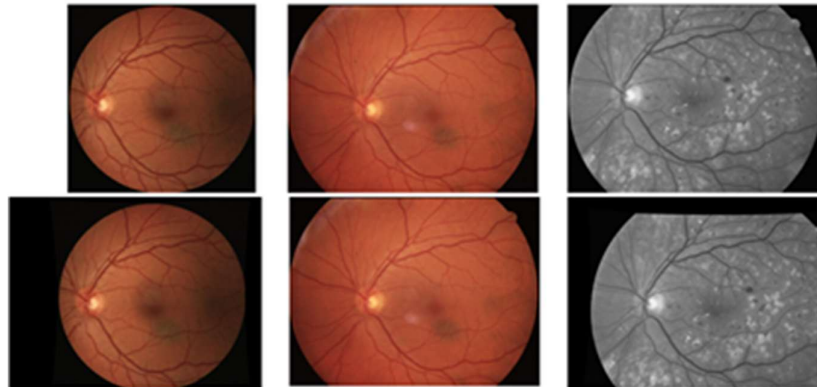


Figure 9. The result of the image registration of the retinal image series. The top row depicts the original image series. The bottom row presents the images after the registration.

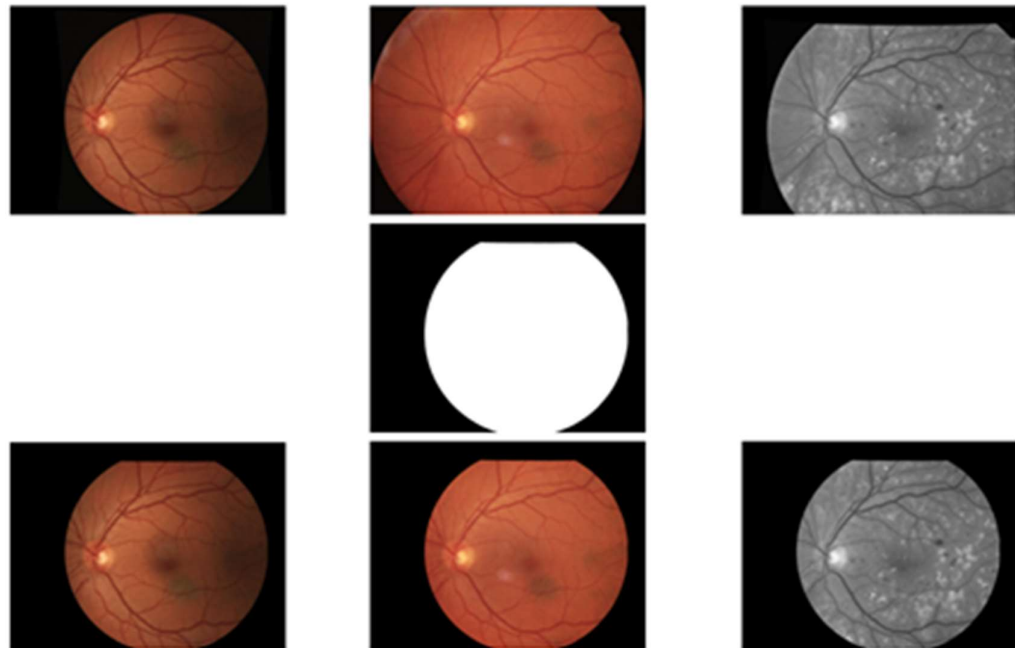


Figure 10. The result of the image cropping. The top row depicts the original image series, from left to right. The image in the middle row is the pixel mask that was obtained by the intersection of the pixel masks from the original images and then applied to them. The bottom row presents the image series after the application of the pixel mask.

The result of image registration is such transformation of the images that their contents align well. The next step after performing the image registration is cropping the images, preserving only the parts covered by all the images of the sequence, as illustrated in Figure 10. The resulting images already allow a visual assessment of differences within the series.

4.2.3 Illumination correction

4.2.3.1 Overview

The images from the dataset differ not only by geometrical properties such as positioning of the imaging target or optics parameters. Another important aspect which may severely interfere with the longitudinal analysis is related to the image colors: some of the images even from the same series tend to contain different color distributions to depict the same objects. Such changes may be due to complex medical reasons, but the most apparent reason in the case of the target dataset is the usage of the different imaging equipment at different time points and the possible variance of lighting conditions [20]. Consider Figure 11 which illustrates the issue.



Figure 11. An example of two images from two different time points with apparently different coloring.

The difference in color is an important obstacle for image series processing. Namely, it obstructs the process of change detection between two images: along with semantically important changes such as newly appeared lesions, a lot of insignificant areas can also be detected as changed only due to the change of color in the whole image.

There are several possible reasons for the color difference among the set, such as changes in an imaging system or illumination. In this work, two approaches to correct the image appearance are considered: illumination correction and color correction.

The purpose of the illumination correction approach is to compensate for the initial non-uniformity of illumination. In the case of retinal imaging, this non-uniformity is always an issue due to the delicateness of the imaging environment: there are a handful of factors to take into account, such as the retinal camera parameters or the dilation of eye pupil.

The simple solutions to this problem include, for example, usage of color spaces which address information about the illumination, for example, L*a*b* [21], but usually robust illumination correction should be problem-oriented and based on mathematical modelling methods [34]. In the application to the change detection, the thematic literature describes non-linear background correction [35], surface fitting [36], or homomorphic filtering [37].

The advantage of the approach used in this work – Iterative Robust Homomorphic Surface Fitting – lies in its problem-specificity: being based on the approaches of surface fitting and homomorphic filtering, it also utilizes the information about the optic disc and vasculature from the target retinal image. The method is introduced and thoroughly described in the article [6].

The foundation of the method is the following approximation:

$$F(x, y, \lambda) = I(x, y, \lambda) \times R(x, y, \lambda), \quad (2)$$

where F is an observed image, I is an illumination component, R is a reflectance component, x and y are image 2D coordinates, and λ is representing a color channel. The illustration for the components can be observed in Figure 12.

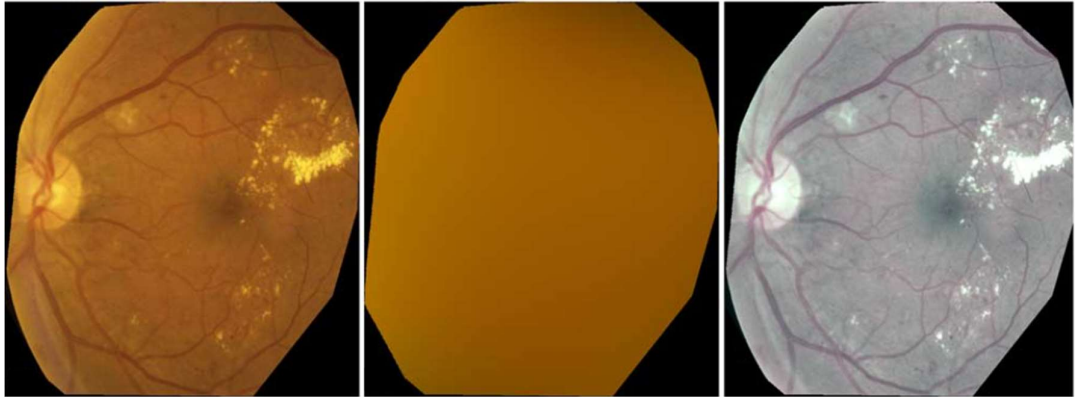


Figure 12. Illustration for the splitting an image to components. The first image is the target image, the central image is its illumination component, and the last image is its reflectance component [6].

The purpose of the method is leveling of the target images to their illumination component. The process of estimation of the components consists of the approximation of the retina by a Lambertian surface. The formation of the illumination component relies on smooth and gradual illumination change, while a rapid intensity change marks the reflectance component.

An important condition of this method consists of excluding of some of the retinal image areas as optic disc, macula, vessels, pathologies, and imaging artifacts during the estimation of the illumination component. This condition implies important features of the implementation since it declares the necessity of preliminary segmentation of these areas, either automatic or manual.

4.2.3.2 Application to the target dataset

Figure 13 demonstrates the application of the illumination correction technique to a retinal image. It is worth to underline that this algorithm perform based only on a single image, and, if applied to several images, it yields conceptually the same result for any retinal image.



Figure 13. The application of illumination correction. The first image is an original image of a time sequence. The second picture is a manually created mask for the vasculature, macula, and optic disc. The third picture is the resulting retinal image with the normalized illumination.

In this case, the mask was drawn manually, as the automatic segmentation of the important areas of the retina is both algorithmically and computationally challenging task to be performed on the dataset. Although later the vasculature segmentation method would be introduced and utilized, the segmentation of the other regions was left out of the scope of this thesis.

4.2.4 Color correction

4.2.4.1 Overview

The purpose of color correction methods is to eliminate the variation of color ranges between images. The approach of histogram specification was suggested as the best reference-based color correction method [38]. The histogram of a grayscale image may be described as a discrete function $h(r_k) = n_k$, where r_k is a k^{th} gray level, and n_k is the number of pixels with this value [21].

The histogram equalization method maps the histogram to the uniform distribution, thus spreading the intensity values over the whole dynamic range and making the image contrast higher. The approach of histogram specification generalizes this case, allowing to map the colors of a given image not only to the uniform distribution but to practically any distribution, namely, the one of the target image.

This approach is originally described for the grayscale images. The simplest approach to the specification of color images is specification of histograms corresponding to the color channels. Consider Figure 14 for the illustration.



Figure 14. The demonstration of color transform by histogram specification. The top row depicts the original images. The bottom row presents the same images with their color ranges specified according to the other image [39].

In the context of automatic diabetic retinopathy detection, it was stated that, even though the color correction improves visualization, it mixes the initial color distribution in an undesirable way [34]. The loss of the underlying information may indeed impact a classification process, but if a study targets the longitudinal information among the images, such as difference among them, the result can eventually remain beneficial.

4.2.4.2 Application to the target dataset

Figure 15 demonstrates the application of color correction to a pair of images from a single series. It is worth to note the effect which can be found in the last image in Figure 15: at the borders of the ellipse, the pixels do not contain the red component, and only green and blue are preserved. It may be due to the incapability of the method to map the information of a channel into another histogram, and the reason may be the prevalence of certain colors on the image. For instance, retinal images, mostly containing the tones of red, can be compared the images in Figure 14, rich in colors. This aspect must be paid special attention to as such mapping failures may lead to inadequate results during the longitudinal processing.

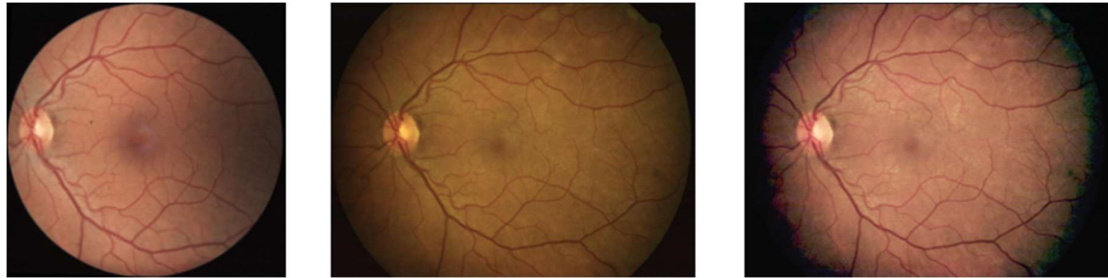


Figure 15. The application of color correction. The first two images are the images of the same series but with different colorings. The last image is the result of the specification of the histogram of the second image to the first image.

4.3 Processing pipeline

After the preprocessing, the images are ready for the analysis of the longitudinal properties of the sequences. The processing of the images involves the following steps:

- Change detection and visualization: this step is the essence of the study of longitudinal series as changes contain the longitudinal information from the data.
- Target segmentation: to simplify the task, it was decided to pursue change detection in a particular target rather than in the images as a whole.
- Change prediction: as it was concluded in the literature review, the machine learning methods are not pertinent to the target dataset. Instead, the morphology approach for interpolation was chosen.

4.3.1 Change detection and visualization

4.3.1.1 Overview

The longitudinal information present in an image series is presented by the changes occurring in its images at the different time points. Thus, the primary tool for the analysis of longitudinal image series is the detection of changes.

A comprehensive survey of change detection algorithms can be found in [40]. One of the most straightforward methods for change detection is subtraction (or differencing) of two successive images [41], [42]. Due to its simplicity, the method is popular and is widely applied in various disciplines.

The immediate result of the image differencing is a difference map representing the absolute values of the differences of pixel intensities between the images. To denote the areas where major differences occur, the difference image may be transformed from grayscale to binary by thresholding.

4.3.1.2 Application to the target database

The described methodology was used to detect and visualize the differences among the longitudinal time series of the target dataset. An example of the result is presented in Figure 16.

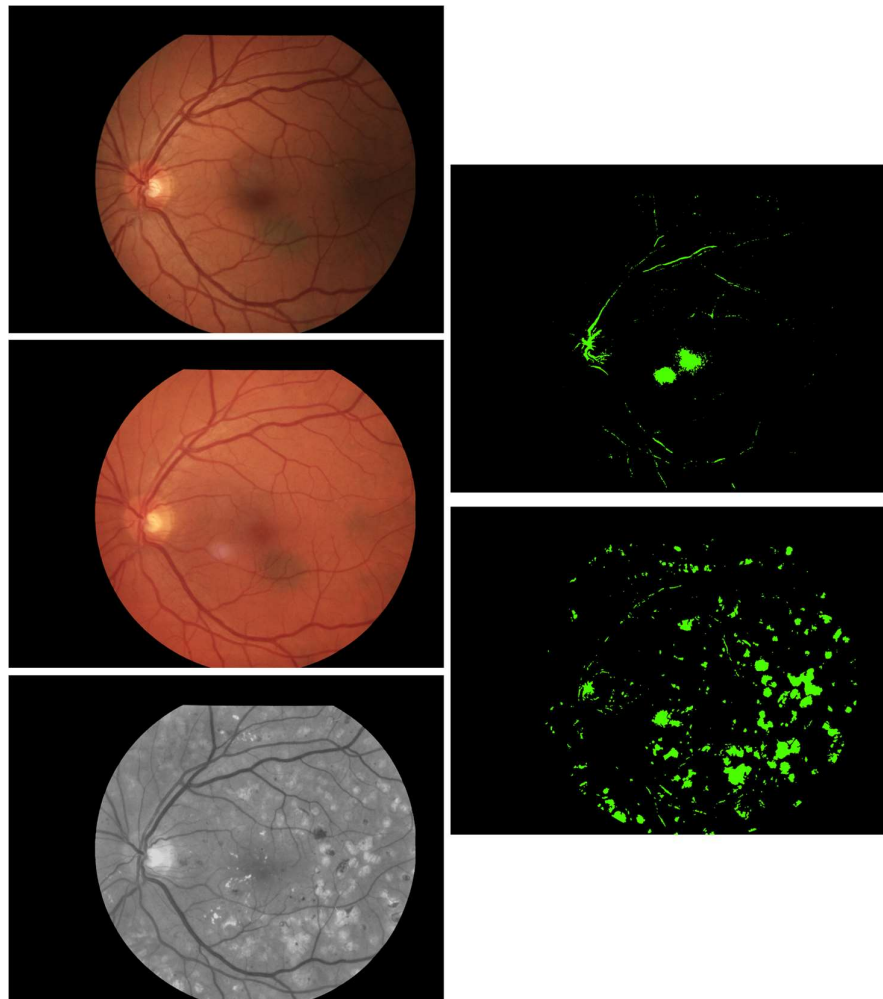


Figure 16. Visualization of differences among a longitudinal image series. The left column depicts the original images. The right column contains the difference images between the corresponding pairs from the left column.

The possible reasoning of the difference images is apparent. The difference image between the first and the second original images mostly outlines the differences in the macula area which truly seems to be darker in the first image. The difference image between the second and the third images depicts the differences justified by the lesions which appeared in the third retinal image.

4.3.2 Vasculature segmentation

4.3.2.1 Overview

The target dataset is assembled out of the photographs taken from patients with diagnosed type 2 diabetes. The disease manifest itself through different abnormalities such as lesions or vasculature changes [20].

The difference maps per se do not reveal changes occurring in the specific areas of interest, and thus the discovered changes can be from various sources. They can not only be caused by different disease signs, but also by artifacts from the preprocessing pipeline (such as image misalignment). The work [6] discusses the source for the classification of the changes, but this is not an approach overtaken in this thesis. Instead, it was decided to choose a specific target present in retinal images and trace the changes occurring in this target. A robust method for segmentation of a target would deprive the system of the necessity to classify the changes and would allow considering the changes only occurring in the area of this target.

Typically, the areas of interest in retinal images are optical disc, fovea, vasculature, or disease abnormalities such as lesions. The topic of segmentation of these targets is well presented in the literature [43]–[47]. In this work, the blood vessel segmentation was selected as the changes in vasculature are prominent to be found through all the target dataset. The work [48] describes a wavelet-based method for the segmentation and its publicly available implementation.

4.3.2.2 Application to the target dataset

Figure 17 presents the result of the blood vessels segmentation from a retinal image. The green channel of the images is utilized since it contains the most relevant data concerning the vasculature structure [44]. It should be noted that the method does not always cope with vasculature segmentation flawlessly. In such cases, some additional steps to improve the

vessel contrast should be overtaken, but they hinder the automatization of the whole processing pipeline as they may confuse the segmentation of the other cases.



Figure 17. The green channel of a retinal image with normalized photometric information and its segmented vasculature.

4.3.3 Morphology-based change prediction

4.3.3.1 Overview

In accordance with the literature review results, it was decided to apply morphological operations for change prediction. Their primary advantage is dependency only on a particular image's contents, and they are simple to implement.

The notion of mathematical morphology is thoroughly explained in [23]. It is a technique commonly used for processing of digital images. The idea of the processing is in the application of some operators to pixels and their neighborhood and transforming their state by these operators. The nature of the operators is based on set theory.

The four primary morphological operators are dilation, erosion, closing, and opening. In this work, the dilation operator and its development to conditional dilation operator are used.

Formally, the dilation operator is defined in the following way [21]:

$$A \oplus S = \{z \mid (\hat{S})_z \cap A \neq \emptyset\}, \quad (6)$$

where A and S are sets in Z^2 , \hat{S} is a reflection of set S ; $(\hat{S})_z$ is translation of set \hat{S} by point $z = (z_1, z_2)$.

In the case of digital imaging, set A is an image, and set S is called a structuring element. It is arbitrarily defined for every application of the dilation operator.

The equation 6 can be illustrated by Figure 18.

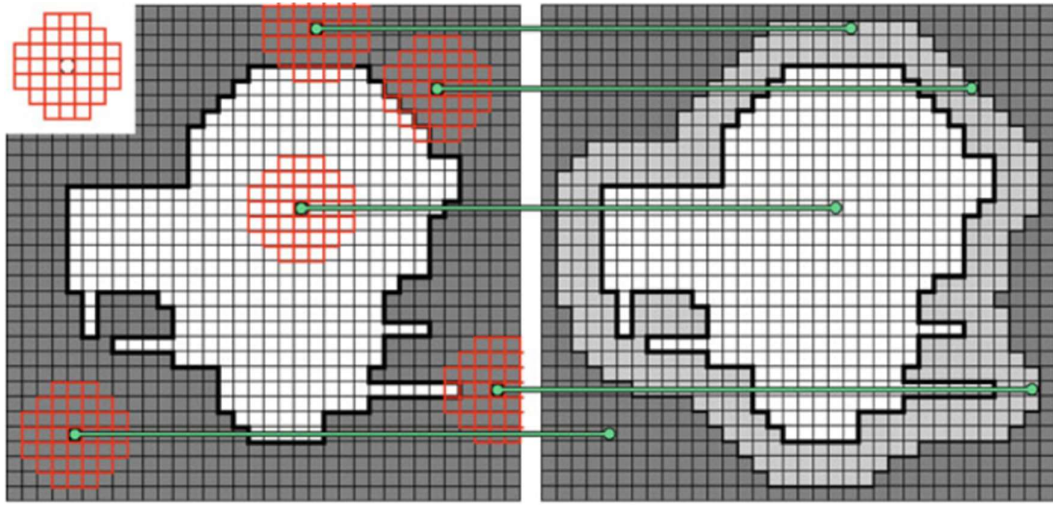


Figure 18. The illustration of an application of the dilation operator. The white pixels represent the set A from the equation 6. The circle-like set of pixels with red borders represents a structuring element S. The green lines indicate the correspondence of locations between the source image pixels where the structuring element was applied and the corresponding pixels of the second image. The gray pixels of the second image are the pixels that were added to the source set A in accordance with the rule described by the equation 6 [23].

In work [15], the *conditional dilation operator* [49] was utilized to perform interpolation. Formally, the operator is written in the following way:

$$B \oplus_A S = (B \oplus S) \cap A, \quad (7)$$

where A, B, and S are sets in Z^2 . In the case of digital imaging, sets A and B are images and set S is a structuring element.

Informally, the operator can be thought of as of applying a stencil represented by set A during a simple dilation operator for set B and restricting the dilation of the target to this stencil. It was proven in [49] that a finite number of conditional dilation operators is required to obtain set A from set B. This statement justifies the efficacy of the conditional dilation operator and a tool for change prediction purposes. For example, in work [15] these sets were interpolation targets depicted on a pair of slices.

4.3.3.2 Implementation

MATLAB does not present ready-to-use functions for the conditional dilation, but it does contain a function for simple dilation. This function – `imdilate()` – was used for implementation of conditional dilation for binary vasculature map images.

As it was mentioned above, the conditional dilation operator can be thought of as of applying a stencil to a dilated image. In other words, the implementation of the method for two given binary images A and B is expressed in two simple operations:

- Performing dilation for image B .
- Removing pixels that are not present in image A from the set of pixels obtained from the dilation.

The first step is implemented through `imdilate()` function. To balance preciseness of the method and the number of the required dilation operations, a disk with the radius of 6 pixels was empirically chosen as the structuring element. The second step is achieved by applying the image A as a mask to the dilation result.

5 EXPERIMENTS AND RESULTS

5.1 Impact of photometric correction techniques on change detection

5.1.1 Color correction

To illustrate the impact of color correction (by histogram matching) on the process of change detection, an image series was registered. After that, the absolute difference between the registered images was taken. For the comparison, a histogram of one image from the pair was specified to the second image, and another absolute difference was computed. Figure 19 illustrates the results of the performed steps.

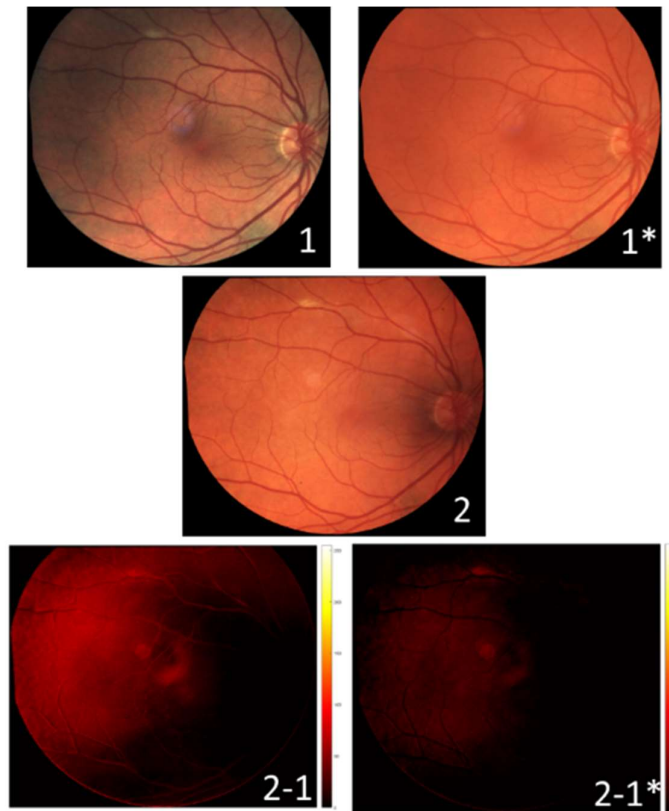


Figure 19. The demonstration of the color correction impact on change detection. The image marked with the digit 1 is the first image of a time series, and the one marked with the digit 2 is the second image. The image marked by the digit 1* with the asterisk is the first image with its histogram specified to the histogram of the second image. The image marked 2-1 depicts the absolute difference between the second and the first image, and the image 2-1* depicts the absolute difference between the second image and the first one with its histogram specified to the second image. For the demonstration purposes, the grayscale difference images 2-1 and 2-1* were color mapped to the red color range: the dark regions denote no intensity difference, while brightly red and yellow mark high and very high intensity difference.

As it can be observed, the difference image 2-1 is affected by the coloring difference: a wide area is colored red, while the corresponding regions have no principal semantical differences. The difference image between the second image and the specified first image also depicts colored area for background differences, even though in a much less magnitude. Experiments demonstrated that the other retinal images series exhibit the same behavior.

The histogram specification method copes with the task of approximating the coloring model of one retinal image to another's, although not perfectly. Still, it is notable that various coloring models treat different semantical areas of the images differently. For instance, in the image 2-1, along with the background, the difference between the blood vessel areas was also detected, but it is eliminated in the image 2-1*.

The histograms of the difference images 2-1 and 2-1* are depicted in Figure 20.

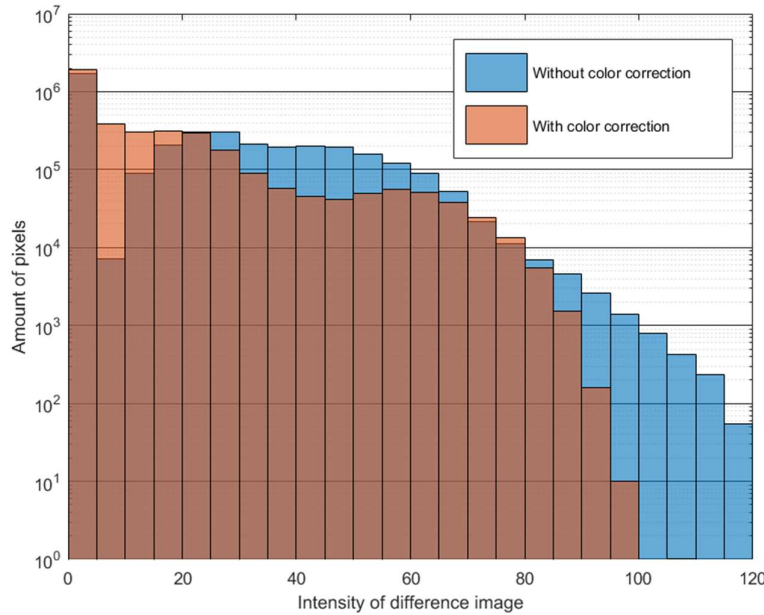


Figure 20. Histogram of intensities in difference images 2-1 and 2-1* presented in Figure 19. A logarithmic scale is used for the axis of the number of pixels.

As it can be observed, the application of color correction reduces a number of pixels with an average intensity which were standing for the difference in coloring, transferring them to the minimum difference.

5.1.2 Illumination correction

A series of experiments similar to the case of color correction was performed using the illumination correction algorithm. As this approach is not reference-based, each image after registration was normalized to the illumination and the reflectance components were obtained. The results of the experiment are illustrated in Figure 21.

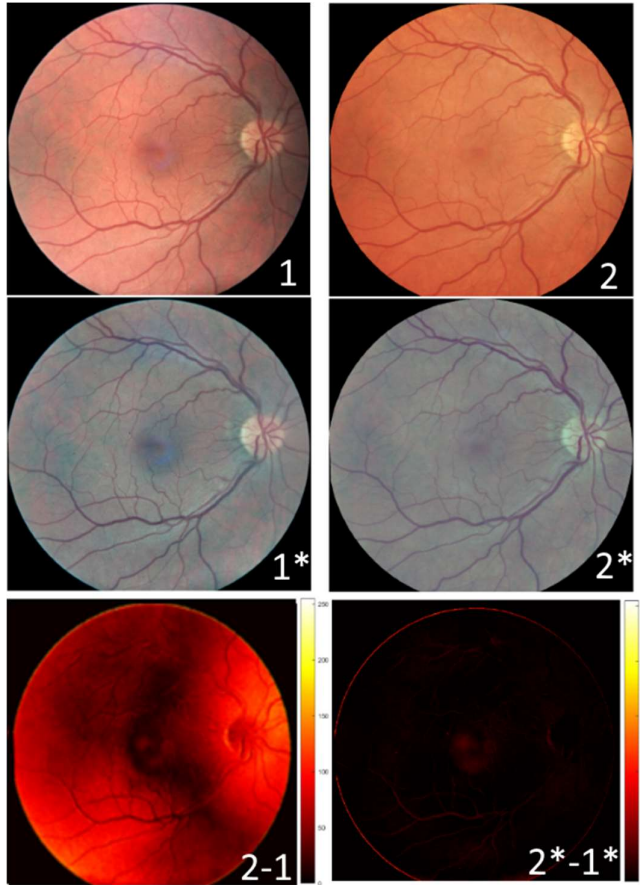


Figure 21. Demonstration of the illumination correction impact. the digit 1 denotes the first image; 2 – the second image; 1^* – the first image with normalized illumination; 2^* – the second image with normalized illumination; $2-1$ – the color mapped grayscale image depicting difference between the original images; 2^*-1^* – the color mapped grayscale image depicting difference between the images with illumination correction.

As it can be observed, the image pair 1 and 2 suffers from the same problem of coloring difference as was the pair from the previous experiment. This fact impacted the difference image $2-1$. However, at the same time, the difference 2^*-1^* depicts a radically different result: the difference between the flat regions is almost completely eliminated, and the difference is shown only in the areas with actual semantic structures such as vasculature.

Figure 22 presents the histograms of the difference images. The histograms demonstrate the considerable improvement of the achievement from the color matching experiment: on the histogram of the image with the illumination correction, the intensities from the middle (supposedly the ones responsible for the flat color difference) are redistributed to the edges, providing a good contrast to the image and denoting only semantically important differences.

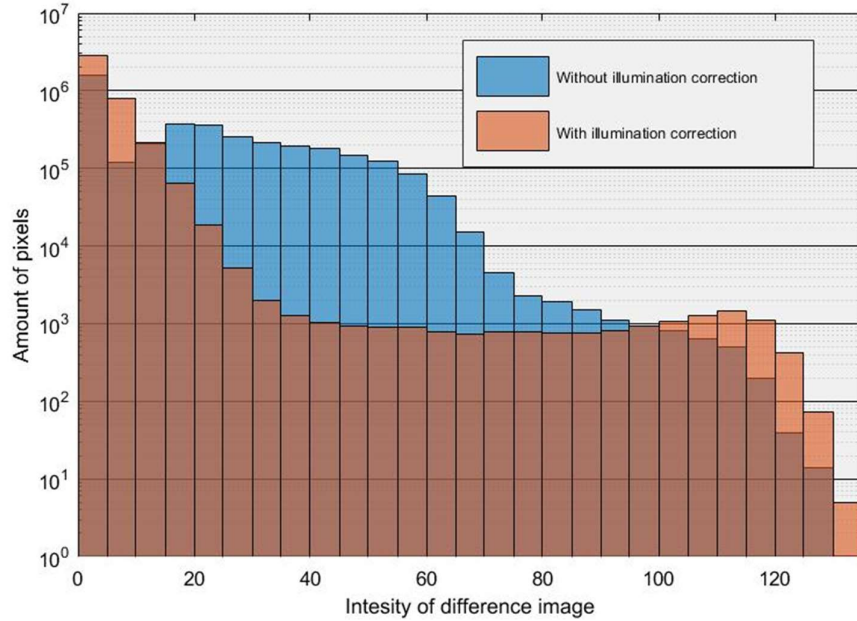


Figure 22. Histogram of intensities on difference images 2-1 and 2*-1* presented in Figure 21. A logarithmic scale is used for the axis of the number of pixels.

5.1.3 Color correction combined with illumination correction

After the described experiments, an additional step was taken which was the application of histogram specification to the reflectance components after the illumination correction. The histograms of the obtained difference images are presented in Figure 23. As it can be observed, the additional application of color correction does not yield as an apparent result as it was demonstrated in Figure 22. Still, the color correction technique does compensate the intensity value for a small number of pixels. The color correction could be used for supporting the illumination correction, but the technique does not seem to be reliable to preserve local texture information which in some cases could be valuable.

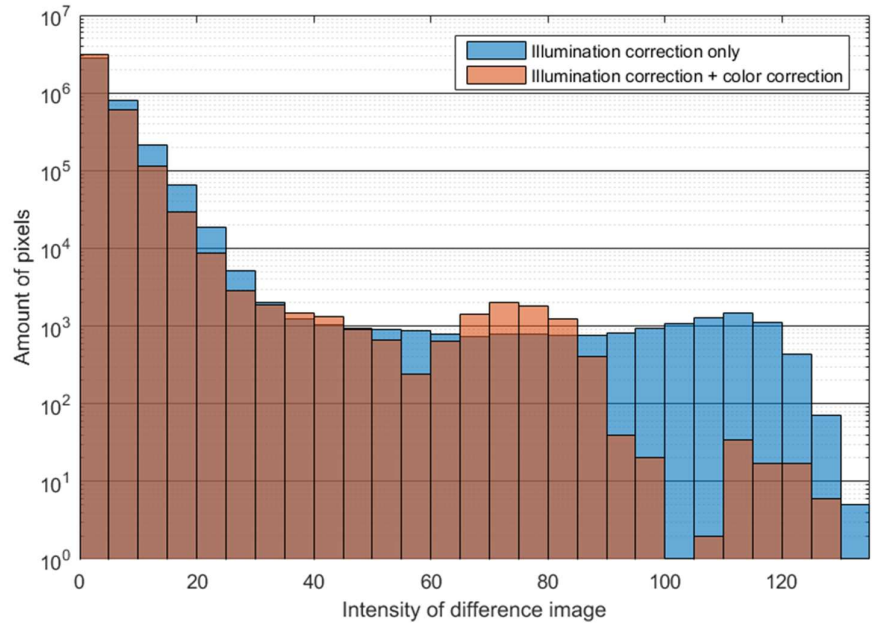


Figure 23. Histogram of intensities on difference image between images 2-1 and 2*-1* from Figure 21, and on difference image between these images with the image 1* specified to image 2*. The axis for a number of pixels has a logarithmic scale.

5.2 Morphology-based change prediction

Consider Figure 24 presenting an example of a setup for the experiments. The experiments targeted the manually picked subareas of vasculature maps like the one outlined by a red ellipse in the bottom-right image of Figure 24. The example is presented in Figure 25. The figure contains the subareas of vasculature maps from retinal images successive in a longitudinal series and a difference map between them. As it can be observed, the vasculature from the latter image apparently becomes thicker.

The application of morphology-based approach allows predicting the changes happening between the images picked from the target dataset. Figure 26 presents an example of the application of the conditional dilation-based prediction for change prediction purposes.

The image marked as ‘I’ denotes the initial setup for conditional dilation. The white area depicts the part of vasculature segmented from the first image of the series which is also depicted in the first image of Figure 25. The green area is the difference between this vasculature and vasculature of the second image.

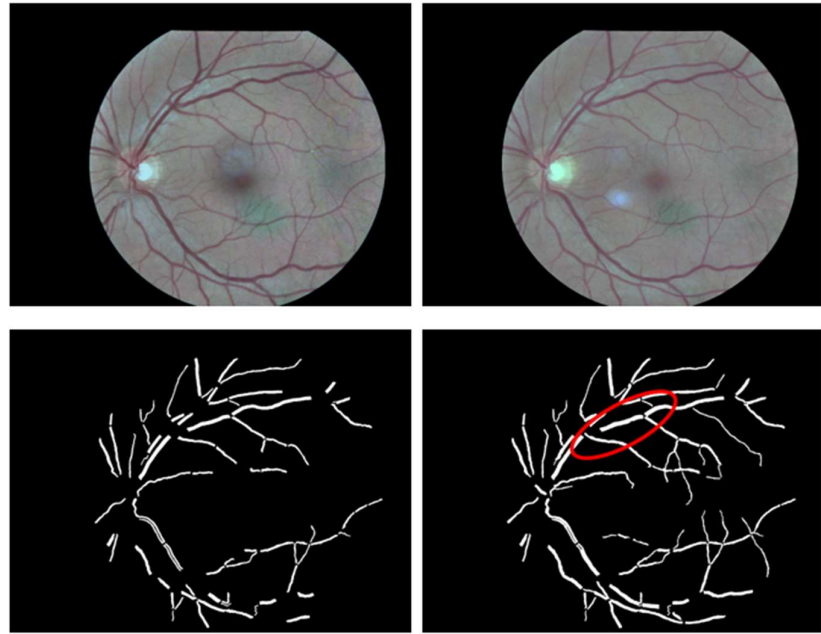


Figure 24. An example of two preprocessed images and segmented vasculatures. The top row presents a pair of preprocessed retinal images. The bottom row depicts the result of the vasculature segmentation algorithm performed on each image. The red ellipse encircles the area used for the further demonstration of the conditional dilation method.

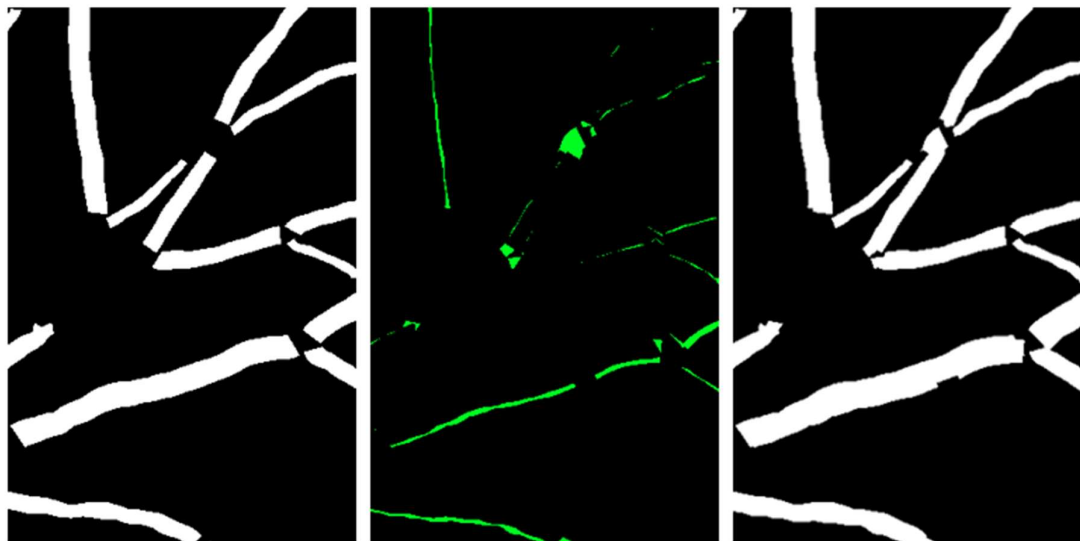


Figure 25. An example of subareas of vasculature masks from the first and the last images of a time series. The image in the center depicts the difference between the last and the first image.

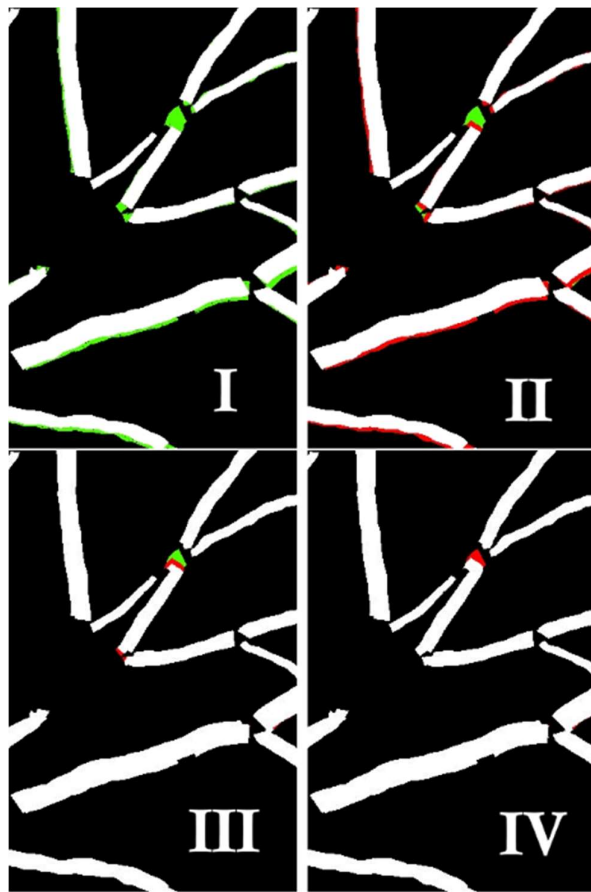


Figure 26. An example of the conditional dilation application. The images depict changes occurring in the images during conditional dilation. The white area is the vasculature segmented from the first image of a time series. The green area is the difference between the vasculature segmented from the last image and the one segmented from the first image. The red area is the pixels produced by conditional dilation applied to the first image.

The images marked as ‘II’, ‘III’, and ‘IV’ depict the attempts of application of conditional dilation operation to the base stage I. Ten conditional dilation operations were applied between two consequent stages. The red area denotes the pixels that were newly added as a result of the morphology operations, and the green area depicts the difference left to fill in order to morph the initial image to the vessels map from the second image. In the last stage, this difference is filled completely, so the morphing is complete.

For this conditional dilation application, the same structural element in the form of a disc with the radius of 6 pixels was used. It is apparent that, for the chosen target of the vasculature, the morphology-based interpolation method could be used to emulate the change prediction between two target images and through the time series of three images.

5.3 Estimation of change pace

It was demonstrated that the mathematical morphology is a reasonable tool for handling change prediction problem in relation to blood vessels.

To compare the rate of change occurrence in a series, it was decided to select areas of retinal images which contained only plain and simple parts of the vasculature, that is, straight segments of a single blood vessel. The areas containing curvatures or intersections with other vessels were excluded from consideration to simplify the experiment. The example of such areas and corresponding binary image of the blood vessels is presented in Figure 27.

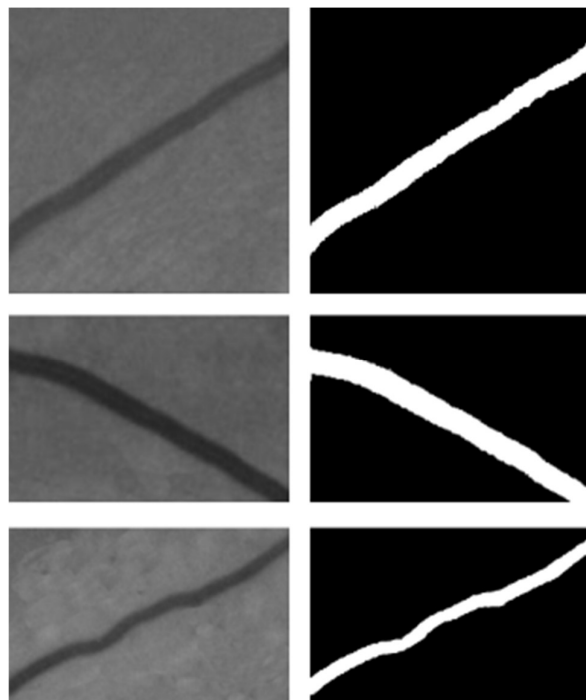


Figure 27. Examples of simple blood vessel areas of retinal images and their binary counterparts obtained through vasculature segmentation.

Using the vasculature segmentation technique, the subregions of the target images were manually selected. Eventually, only about a half of the original image set was selected for the experiment, as not all the original images contained areas as simple as described above. The final set of images included 315 images, as not all the selected areas exhibited the phenomena of blood vessel widening.

In order to characterize the rate of vessel widening, it was decided to compare the number of conditional dilation iterations, described in the previous section, to morph the first image of the series to the second, and the second image to the third one, as was demonstrated in the previous section. The morphology structuring element remained to be a disk with the radius of 6 pixels.

Consider Figure 28 depicting the pipeline of the experiment.

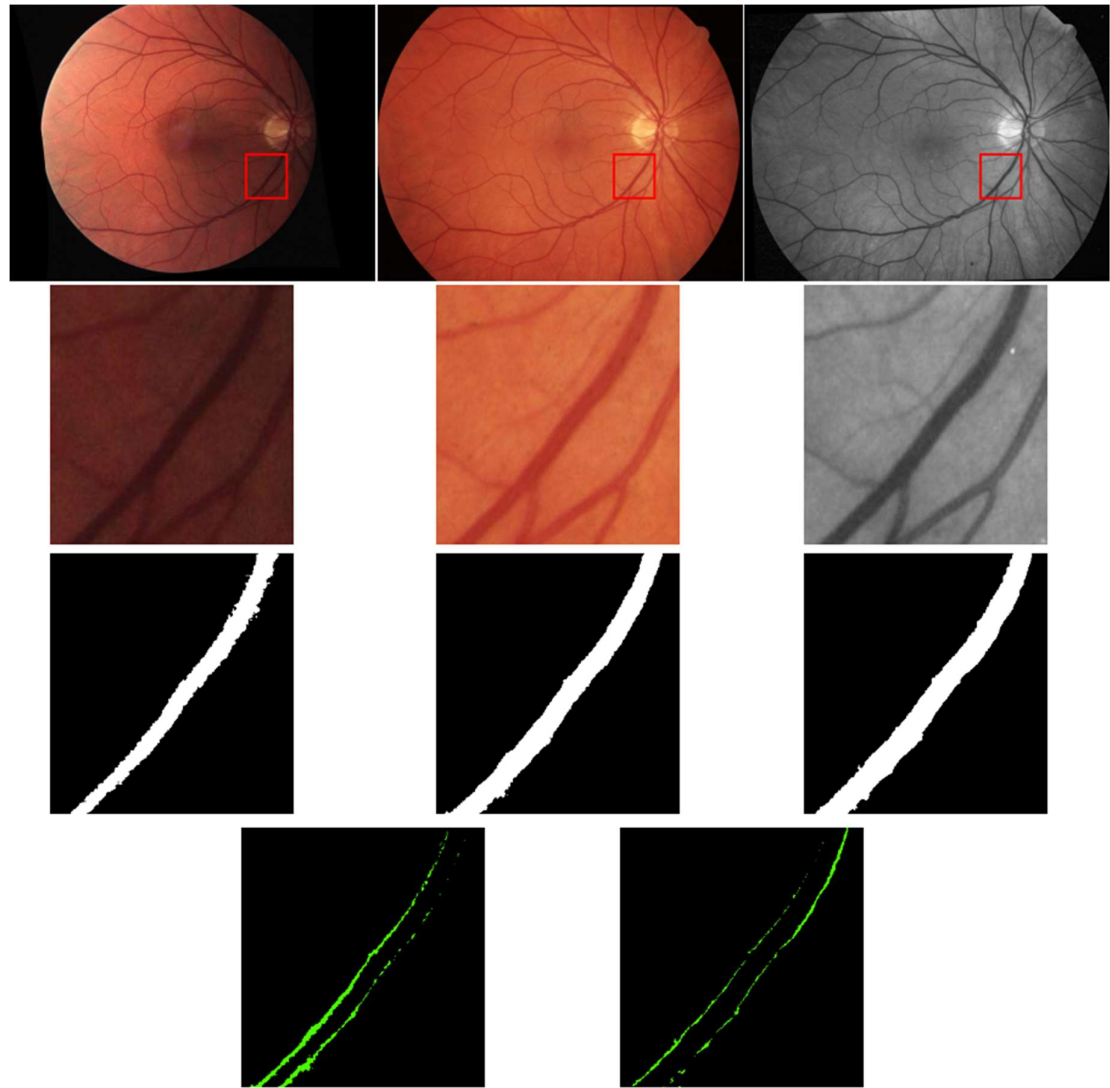


Figure 28. A demonstration of the processing pipeline conducted in the experiments. The first row depicts the original registered image series. The red rectangle encircles the vessel area considered in the experiment. The second row depicts the considered vessel area. The third row depicts the corresponding binary vessel images (as in Figure 27). The last row depicts the differences between the pairs of binary images of the vessels which is required to be filled by the morphology operations.

In Figure 28, the growth of the vessel from the first time point to the second time point was 23% of the overall volume of the vessel segmented from the first time point. The growth from the second to the third time point was 16% of the volume of the vessel segmented from the second time point. The conditional dilation operator was applied three times to compensate the difference between the time points. Even though the difference between the second and the third time point is less in volume than the difference between the first and the second time point, it still required the same number of the morphology operations due to unevenness of the width growth along the vessel.

Among the selected fragments, 58 image series out of 102 demonstrated that if they contain a widening blood vessel, the difference between their time points can be filled by the same number of the conditional morphology operators (three operators in the case of this experiment), meaning that its width changes roughly by the same value from the first time point to the second, and from the second to the third one. The other series exhibit such vessel widening that it requires a different number of the operators to compensate the difference between time points. Furthermore, 28 of such image series demonstrated no change in vessel width between the first and the second time point, and some notable change occurred only between the second and the third time point.

5.4 Discussion

5.4.1 Photometric correction

The work [6] describes only the usage of the illumination correction algorithm, but in this thesis, it was also decided to test the applicability of the color correction approach. The performed experiments demonstrated the viability of the both approaches for the task of eliminating of semantically insignificant differences among the images. Still, it was eventually decided to proceed with the usage of the illumination correction approach only.

In application to medical image processing, the histogram specification approach could be characterized as naïve since it operates only on the color information and provides the solution regardless of the actual contents of the images. It may lead to possible information losses as the corrections can be applied inadequately to medically important areas such as lesions.

Furthermore, the design of the method allows only two images to be specified, and specification of a series of three and more images would require additional steps. This lack of universality may be inconvenient for the analysis of big sets of long image series.

On the other hand, the illumination correction approach attempts to model the illumination environment and provides normalized images with no dependency on the other images of a series. This method is both reliable concerning sensitive medical information and universal in application to large image sets. Additionally, the experiments demonstrated that this method provides a better contrast of pixel intensities in semantically important areas.

As it was demonstrated, the photometric correction algorithms crucially impact the change detection. At the same time, the part of these algorithms in morphology-based change prediction was not as important since it depends only on the vasculature segmentation of a single image.

5.4.2 Change prediction

For the change prediction, the morphology-based approach was used. It is conceptually simple and easy to apply, as it operates on the information from the target image only. The trade-off is an empiric nature of results, with no robust theoretical grounds.

The results obtained in morphology-based change prediction may be used for the interpolation between two time points. If a time series possesses the regularity in change occurrence pace, it may be relatively safe to use this technique for the extrapolation. Even though the obtained results would be very likely not to predict the exact shape of a blood vessel, they could be useful for the prediction of quantitative values such as area coverage.

To the author's opinion, the results achieved by the morphology-based techniques are not reliable to judge the nature of blood vessels width change as it is. The observed regularities in width change behavior are too blunt and too empiric to be used for as exacting area as medicine. However, these regularities may indicate a hidden potential for the blood vessel imaging to be a target for machine learning, should there be enough data to design it.

5.4.3 Notes on desired features of the longitudinal retinal image datasets

The target dataset's nature has severely impacted the work on it. Primarily, even though the dataset contains several pictures for patients, taken at different time points, the number of these time points is not sufficient for machine learning application. It is the key difference from the dataset discussed in [8]. Additionally, as the author of the work has no relevant knowledge of medicine, it was unclear how to choose the study target in time series.

Another important feature of the dataset is the lack of specified parameters of imaging systems used for retina image capture. Had the dataset been supplemented with the information like camera calibration, it would have changed the image registration process of the preprocessing pipeline. Namely, the transformation model could be simplified from the lens distortion to quadratic, as recommended in [32].

Consequently, it would be desired for a data set of longitudinal retinal image series to possess the qualities mentioned above, namely, specified information about imaging system and a number of time points in a series sufficient for the application of machine learning.

6 CONCLUSIONS

This thesis is dedicated to the analysis of the longitudinal retinal image series. During the work, the target dataset was studied and prepared for the processing. The images of the dataset were preprocessed. Both image-wise and series-wise preprocessing techniques were studied and applied.

The longitudinal image analysis techniques were considered in the context of the target dataset. On the basis of the assembled longitudinal preprocessing pipeline, a morphology-based technique was proposed as a change prediction method for blood vessels in the images of the target dataset.

An experiment was conducted to demonstrate the efficacy of the method for studying the longitudinal properties of the dataset. The purpose of the experiment was to establish possible regularities in the rates of the change occurrences in blood vessels throughout the dataset series.

The experiment demonstrated that about 56% of the image sequences contain blood vessel regions which widen with approximately the same rate between consequent time points. The results could indicate a possible resource for a machine learning study of the considered dataset, should it be organized with consideration of the formulated requirements.

REFERENCES

- [1] E. Mensah and E. Kohner, "Diagnosis and management of diabetic retinopathy," *Topic Endocrinol*, vol. 19, pp. 14–8, 2002.
- [2] R. J. Tapp *et al.*, "The prevalence of and factors associated with diabetic retinopathy in the Australian population," *Diabetes care*, vol. 26, no. 6, pp. 1731–1737, 2003.
- [3] G. S. Scotland *et al.*, "Costs and consequences of automated algorithms versus manual grading for the detection of referable diabetic retinopathy," *British Journal of Ophthalmology*, vol. 94, no. 6, pp. 712–719, 2010.
- [4] P. Soliz, M. P. Wilson, S. C. Nemeth, and P. Nguyen, "Computer-aided methods for quantitative assessment of longitudinal changes in retinal images presenting with maculopathy," in *Medical Imaging 2002*, 2002, pp. 159–170.
- [5] L. Schardosim, J. Scharcanski, D. D. Santos Jr, and J. Stuchi, "Motion detection in infrared retinal image sequences," in *Instrumentation and Measurement Technology Conference (I2MTC), 2011 IEEE*, 2011, pp. 1–5.
- [6] H. Narasimha-Iyer *et al.*, "Robust detection and classification of longitudinal changes in color retinal fundus images for monitoring diabetic retinopathy," *Biomedical Engineering, IEEE Transactions on*, vol. 53, no. 6, pp. 1084–1098, 2006.
- [7] H. Narasimha-Iyer, A. Can, B. Roysam, H. L. Tanenbaum, and A. Majerovics, "Integrated analysis of vascular and nonvascular changes from color retinal fundus image sequences," *Biomedical Engineering, IEEE Transactions on*, vol. 54, no. 8, pp. 1436–1445, 2007.
- [8] X. Chen, R. Summers, and J. Yao, "FEM-based 3-D tumor growth prediction for kidney tumor," *Biomedical Engineering, IEEE Transactions on*, vol. 58, no. 3, pp. 463–467, 2011.
- [9] O. Clatz *et al.*, "Realistic simulation of the 3-D growth of brain tumors in MR images coupling diffusion with biomechanical deformation," *Medical Imaging, IEEE Transactions on*, vol. 24, no. 10, pp. 1334–1346, 2005.
- [10] L. Pei, S. Reza, and K. M. Iftekharuddin, "Improved brain tumor growth prediction and segmentation in longitudinal brain MRI," in *Bioinformatics and Biomedicine (BIBM), 2015 IEEE International Conference on*, 2015, pp. 421–424.
- [11] H. Wang and P. A. Yushkevich, "Multi-atlas segmentation without registration: a supervoxel-based approach," in *International Conference on Medical Image Computing and Computer-Assisted Intervention*, 2013, pp. 535–542.
- [12] A. Kummert and M. Schnitzler, "Kalman filter and 3 D warping based image prediction for realtime computer generated image sequences.,," in *IASTED International Conference on Signal Processing, Pattern Recognition, and Applications*, 2003, pp. 1–5.
- [13] R. W. Curwen, A. A. Amini, J. S. Duncan, and F. Lee, "Tracking vascular motion in X-ray image sequences with Kalman snakes," in *Computers in Cardiology 1994*, 1994, pp. 109–112.
- [14] O. Chutatape, L. Zheng, and S. M. Krishnan, "Retinal blood vessel detection and tracking by matched Gaussian and Kalman filters," in *Engineering in Medicine and Biology Society, 1998. Proceedings of the 20th Annual International Conference of the IEEE*, 1998, vol. 6, pp. 3144–3149.
- [15] A. B. Albu, T. Beugeling, and D. Laurendeau, "A morphology-based approach for interslice interpolation of anatomical slices from volumetric images," *Biomedical Engineering, IEEE Transactions on*, vol. 55, no. 8, pp. 2022–2038, 2008.

- [16] “REVIEW - A Reference Data Set for Retinal Vessel Profiles.” [Online]. Available: <http://reviewdb.lincoln.ac.uk/REVIEWDB/Download.aspx>. [Accessed: 01-Jun-2016].
- [17] “DRIVE: Digital Retinal Images for Vessel Extraction | Computer Vision Online.” [Online]. Available: <http://www.computervisiononline.com/dataset/1105138662>. [Accessed: 31-May-2016].
- [18] “The STARE Project.” [Online]. Available: <http://www.ces.clemson.edu/~ahover/stare/>. [Accessed: 31-May-2016].
- [19] “DIARETDB1 - STANDARD DIABETIC RETINOPATHY DATABASE.” [Online]. Available: <http://www.it.lut.fi/project/imageret/diaretbdb1/>. [Accessed: 31-May-2016].
- [20] V. Kalesnykiene, I. Sorri, R. Voutilainen, M. Uusitupa, L. Niskanen, and H. Uusitalo, “The effect of glycaemic control on the quantitative characteristics of retinopathy lesions in patients with type 2 diabetes mellitus: 10-year follow-up study,” *Graefe’s Archive for Clinical and Experimental Ophthalmology*, vol. 247, no. 3, pp. 335–341, 2009.
- [21] R. C. Gonzalez and R. E. Woods, *Digital image processing*, 3rd ed. Pearson, 2007.
- [22] M. C. Motwani, M. C. Gadiya, R. C. Motwani, and F. C. Harris, “Survey of image denoising techniques,” in *Proceedings of GSPX*, 2004, pp. 27–30.
- [23] B. G. Batchelor, *Machine Vision Handbook*. Springer, 2012.
- [24] R. Szeliski, *Computer vision: algorithms and applications*. Springer Science & Business Media, 2010.
- [25] D. L. Hill, P. G. Batchelor, M. Holden, and D. J. Hawkes, “Medical image registration,” *Physics in medicine and biology*, vol. 46, no. 3, p. R1, 2001.
- [26] L. G. Brown, “A survey of image registration techniques,” *ACM computing surveys (CSUR)*, vol. 24, no. 4, pp. 325–376, 1992.
- [27] B. Zitova and J. Flusser, “Image registration methods: a survey,” *Image and vision computing*, vol. 21, no. 11, pp. 977–1000, 2003.
- [28] J. A. Maintz and M. A. Viergever, “A survey of medical image registration,” *Medical image analysis*, vol. 2, no. 1, pp. 1–36, 1998.
- [29] L. Laaksonen, E. Claridge, P. Falt, M. Hauta-Kasari, H. Uusitalo, and L. Lensu, “Comparison of image registration methods for composing spectral retinal images,” 2014.
- [30] G. Yang, C. V. Stewart, M. Sofka, and C.-L. Tsai, “Registration of challenging image pairs: Initialization, estimation, and decision,” *Pattern Analysis and Machine Intelligence, IEEE Transactions on*, vol. 29, no. 11, pp. 1973–1989, 2007.
- [31] D. G. Lowe, “Distinctive image features from scale-invariant keypoints,” *International journal of computer vision*, vol. 60, no. 2, pp. 91–110, 2004.
- [32] C. V. Stewart, C.-L. Tsai, and B. Roysam, “The dual-bootstrap iterative closest point algorithm with application to retinal image registration,” *Medical Imaging, IEEE Transactions on*, vol. 22, no. 11, pp. 1379–1394, 2003.
- [33] “Transformation Format.” [Online]. Available: <http://www.cs.rpi.edu/research/groups/vision/gdbicp/exec/transform.html>. [Accessed: 07-Sep-2016].
- [34] T. Kauppi, *Eye fundus image analysis for automatic detection of diabetic retinopathy*. Lappeenranta University of Technology, 2010.
- [35] M. J. Carlotto, “Nonlinear background estimation and change detection for wide-area search,” *Optical Engineering*, vol. 39, no. 5, pp. 1223–1229, 2000.
- [36] K. Skifstad and R. Jain, “Illumination independent change detection for real world image sequences,” *Computer Vision, Graphics, and Image Processing*, vol. 46, no. 3, pp. 387–399, 1989.

- [37] R. Guillemaud, “Uniformity correction with homomorphic filtering on region of interest,” in *Image Processing, 1998. ICIP 98. Proceedings. 1998 International Conference on*, 1998, vol. 2, pp. 872–875.
- [38] K. A. Goatman, A. D. Whitwam, A. Manivannan, J. A. Olson, and P. F. Sharp, “Colour normalisation of retinal images,” in *Proceedings of Medical Image Understanding and Analysis*, 2003, pp. 49–52.
- [39] M. Grundland and N. A. Dodgson, “Color histogram specification by histogram warping,” in *Electronic Imaging 2005*, 2005, pp. 610–621.
- [40] R. J. Radke, S. Andra, O. Al-Kofahi, and B. Roysam, “Image change detection algorithms: a systematic survey,” *Image Processing, IEEE Transactions on*, vol. 14, no. 3, pp. 294–307, 2005.
- [41] P. L. Rosin, “Thresholding for change detection,” *Computer vision and image understanding*, vol. 86, no. 2, pp. 79–95, 2002.
- [42] P. L. Rosin and E. Ioannidis, “Evaluation of global image thresholding for change detection,” *Pattern Recognition Letters*, vol. 24, no. 14, pp. 2345–2356, 2003.
- [43] A. Osareh, M. Mirmehdi, B. Thomas, and R. Markham, “Automated identification of diabetic retinal exudates in digital colour images,” *British Journal of Ophthalmology*, vol. 87, no. 10, pp. 1220–1223, 2003.
- [44] C. Sinthanayothin, J. F. Boyce, H. L. Cook, and T. H. Williamson, “Automated localisation of the optic disc, fovea, and retinal blood vessels from digital colour fundus images,” *British Journal of Ophthalmology*, vol. 83, no. 8, pp. 902–910, 1999.
- [45] A. Hoover and M. Goldbaum, “Locating the optic nerve in a retinal image using the fuzzy convergence of the blood vessels,” *Medical Imaging, IEEE Transactions on*, vol. 22, no. 8, pp. 951–958, 2003.
- [46] R. Chrátek, M. Wolf, K. Donath, G. Michelson, and H. Niemann, “Optic disc segmentation in retinal images,” in *Bildverarbeitung für die Medizin 2002*, Springer, 2002, pp. 263–266.
- [47] G. D. Joshi, J. Sivaswamy, and S. R. Krishnadas, “Optic disk and cup segmentation from monocular color retinal images for glaucoma assessment,” *Medical Imaging, IEEE Transactions on*, vol. 30, no. 6, pp. 1192–1205, 2011.
- [48] P. Bankhead, C. N. Scholfield, J. G. McGeown, and T. M. Curtis, “Fast retinal vessel detection and measurement using wavelets and edge location refinement,” *PloS one*, vol. 7, no. 3, p. e32435, 2012.
- [49] J. Serra, *Image analysis and mathematical morphology*. Academic press, 1982.